RGNZ/MGPB

Investigating Absorption Effects on Oil Droplets in Enhanced Oil Recovery: A Force Analysis Approach

Rudarsko-geološko-naftni zbornik
(The Mining-Geology-Petroleum Engineering Bulletin)
UDC: 622.2
DOI: 10.17794/rgn.2024.4.8

Original scientific paper

Mohammed A. Samba[1]; Yiqiang Li[2]; Zheyu Liu[3]; Ibrahim A. Amar[4]; Muslim Abdurrahman[5]; Peter O. Anyimah[6]

[1] *College of Petroleum Engineering, China University of Petroleum (Beijing), Beijing 102249, PR China*
[2] *College of Petroleum Engineering, China University of Petroleum (Beijing), Beijing 102249, PR China*
[3] *College of Petroleum Engineering, China University of Petroleum (Beijing), Beijing 102249, PR China.*
[4] *Department of Chemistry, Faculty of Science, Sebha University, Sebha, Libya*
[5] *Department of Petroleum Engineering, Universitas Islam Riau, Riau, Indonesia*
[6] *College of Petroleum Engineering, China University of Petroleum (Beijing), Beijing 102249, PR China*

Abstract

This research aims to analyze the forces that affect oil droplets to illustrate that augmenting the mass of an oil droplet fosters favorable conditions for interaction between displaced and displacing fluids. This, in turn, impedes the bypassing of the displacing fluid around the oil droplets. In this investigation, the concept of augmenting the mass of an oil droplet is realized through absorption phenomena, employing coated spinel oxide (cobalt ferrite oxide) nanoparticles (CFO NPs). The synthesis of CFO NPs was successfully carried out in the laboratory using a sol-gel technique, followed by coating with a surfactant and lauric acid. The coated spinel oxide NPs underwent characterization using IR, XRD, and XRF techniques. The procedures started with the calculation of capillary force restrictions for small and large oil droplets. Furthermore, practical experiments involving oil droplets on glass plates at a 30° angle were conducted for different scenarios: without water injection, with water injection, and during the "absorption effect" of CFO NPs. The findings revealed that a large oil droplet exhibits lower capillary pressure restrictions compared to a small oil droplet, with a disparity of 0.02 m/s^2. Consequently, it is comparatively easier for large oil droplets to become free than small ones. Moreover, a large oil droplet exhibits faster movement than small oil droplets due to gravitational effects in the absence of any injections. During the water injection scenario, the water droplets were unable to displace the oil droplet; instead, they passed through the passage beside and above the oil droplet consistently with an increase in the amount of water droplets. However, in the coated CFO NPs scenario, absorption of the coated CFO NPs onto the oil droplet was observed. This resulted in the aggregation of oil molecules, augmenting the gravity of the oil droplet and creating favourable conditions for its displacement. Notably, no water bypass beside the oil droplet was observed in this scenario, unlike the water scenario. Additionally, the aggregation of oil molecules induced corner flow, providing conducive conditions for microemulsion formation, altering wettability, modifying residual oil saturation, and enhancing injection performance. Euler's equation was employed to analyse corner flow, indicating that the level of oil deformation increases with the rising rotation velocity, potentially leading to an increased recovery factor.

Keywords:
oil droplet; gravity force; capillary force; corner flow; spinel oxide nanoparticle

1. Introduction

Enhanced oil recovery (EOR) involves altering reservoir properties to increase oil production. These modifications often arise from interactions between the displacing fluid and the reservoir rock, or between the displacing fluid and the displaced fluid. Such alterations can manifest in various ways, including heightened gravitational forces, oil swelling, alterations in wettability, reduced interfacial tension, decreased oil viscosity, and reduced capillary forces (**Green and Willhite, 1998; Samba et al., 2023**).

The capillary force stands out as a pivotal parameter with a significant impact on the recovery factor (**Green and Willhite, 1998; Samba et al., 2023; Agbalaka et al., 2009; Romanuka et al., 2012**). Extensive research studies have delved into this parameter (**Tola et al., 2017; Nobakht et al., 2007; Sun et al., 2017; Rai et al., 2013; Esfe et al., 2020; Rossen and Lu, 1997**). However, the effect of capillary force on EOR requires further investigation to unravel the remaining mysteries.

One intriguing mystery revolves around the interplay between capillary force and gravity force (mass of the

Corresponding author: Mohammed A Samba
e-mail address: Mohammed_samba@yahoo.com

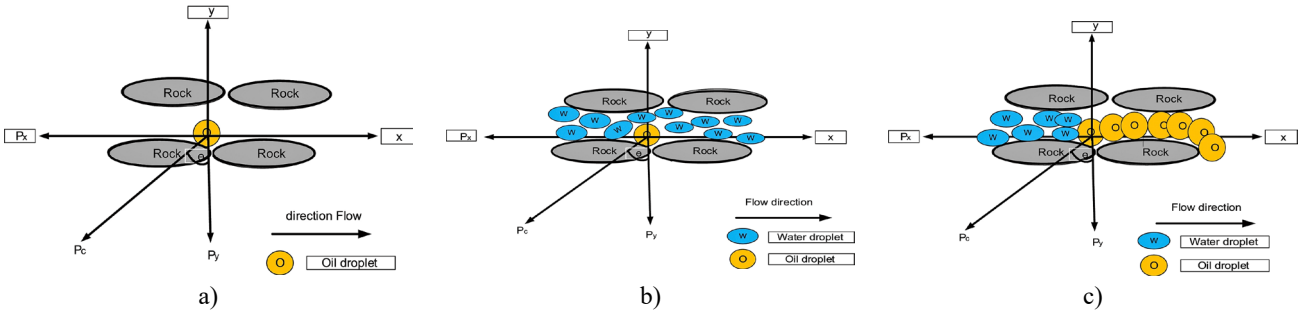

Figure 1: Visualization of the forces exerted on an oil droplet positioned atop a rock surface under various conditions: a) in the absence of injection, b) with water injection, and c) when water injection coincides with an increase in the oil mass (**Samba et al., 2023**)

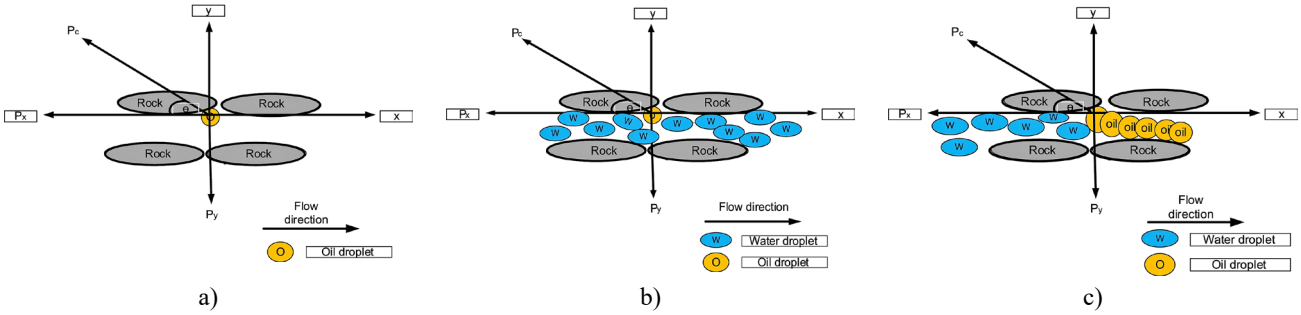

Figure 2: Visualization of the forces influencing an oil droplet when it hangs from the underside of a rock surface, considering three scenarios: a) in the absence of injection, b) with water injection, and c) when water injection accompanies an increase in the oil mass (**Samba et al., 2023**)

oil droplet). A laboratory investigation conducted by Delft University in 2001 delved into the capillary force near a wellbore, comparing it with capillary forces in distant areas. The study unveiled a notable disparity, showcasing that the capillary force near from the wellbore surpasses those in far zones, situated away from the wellbore (**Janssen et al., 2001**). The results have yielded valuable insight, prompting exploration within our current context. In general, the area near the wellbore indicates that a large amount of oil droplets have been produced, and as a result, the pores have become almost empty or contain small oil droplets instead of large oil droplets. Consequently, when the oil droplet size is large, the corresponding capillary force diminishes, while smaller oil droplets yield greater capillary force. Thus, there exists an inverse relationship between capillary force and the weight of the oil droplet. In 2020, Andersen et al. illustrated the impact of capillary force on saturation changes, proposing a graphical representation of saturations versus capillary pressure. This study emphasized the inverse relationship between capillary forces and the mass of the oil droplet (**Andersen, 2020**).

In 2023, an innovative study scrutinized the forces acting upon an oil droplet, namely capillary and gravitational forces. The investigation considered two distinct positions of the oil droplet: situated atop a rock surface and suspended beneath the rock surface. Three injection scenarios were hypothesized, encompassing cases without water injection, with water injection when the oil droplet is small, and with water injection as the mass of the oil droplet increases, as depicted in **Figures 1** and **2**.

The findings illuminated that augmenting the mass of an oil droplet instigates favourable conditions for the synchronization between the displacing and displaced fluids, thereby impeding the injecting fluid from bypassing the displaced fluid (the oil droplet). Moreover, the analysis underscored the substantial role played by the mass of the displaced fluid (oil droplet) in instigating movement when the capillary force is outweighed by the gravitational force. Consequently, the oil droplet can readily advance (**Samba et al., 2023**).

The analysis discussed above constitutes part 1 of this research (**Samba et al., 2023**). A primary hurdle addressed in the preceding study was the methodological challenge of augmenting the mass of the oil droplet subsequent to its analytical validation for enhancing oil recovery. Keeping this in perspective, this work introduces a pioneering method for increasing the mass of an oil droplet, which relies on absorption phenomena.

Numerous materials have the capacity to absorb crude oil, among them CFO NPs, classified as nanoparticle materials. In this investigation, an absorption experiment was conducted utilizing CFO, intended as a sorbent material for oil droplets to augment their mass. The outcomes validate the analysis conducted in part 1 of this research (**Samba et al., 2023**).

The absorption technique has been utilized for oil spill remediation in marine environments (**Amar et al.,**

2021; Amar et al., 2023; Samba et al., 2020). Nevertheless, this approach has not yet been used in the EOR section. This is the first study to open a new window for research in the absorption section to enhance oil recovery, especially in the case of NPs.

2. Materials and methods

To achieve the research goals, several procedures have been employed to synthesize the NPs materials, while others have been used to obtain results from various experimental tests, validating the analysis performed in part 1 of this work (**Samba et al., 2023**). The preparation commenced with the preparation of coated spinel oxide, with a surfactant and lauric acid chosen for coating the spinel oxide. The purpose of coating spinel oxide is to ensure less precipitation and long-distance transport of spinel oxide in the reservoir. Generally, surfactants have proven effective for coating NPs, facilitating their long-distance transport from wells (**Massoud et al., 2022**). Additionally, lauric acid has been demonstrated to coat NPs and prevent their precipitation (**Pradhan et al., 2007**). As mentioned earlier, spinel oxide NPs were selected for use in this study as the primary absorbent material to test the effect of coated spinel oxide NPs on oil droplets, and check whether coating spinel oxide NPs could increase the mass of the oil droplets, and prove that the absorption phenomena can lead to improve the oil recovery. In 2022, Massoud and others suggested that the best method to discover the real effect of implemented NPs materials for researchers is to synthesize or supervise their preparation, rather than ordering them commercially. This step was used to guarantee that no accompanying materials were added to the pure NPs material. Additionally, if there are any accompanying materials in the NPs material, researchers will consider it (**Massoud et al., 2022**). Some studies have reported synthesizing NPs material in the laboratory and implementing those materials in EOR implementations to test their primary effect without any accompanying materials (**Samba et al., 2019**). Therefore, the spinel cobalt ferrite oxide powder was decided to be prepared in the laboratory by following special procedures, as shown in **Figure 3**. The spinel cobalt ferrite oxide powder was prepared in different stages to maintain and control the mixture. In each stage, 10 gm of spinel NPs formula (CFO) $COFe_2O_4$ was prepared using the sol-gel method (**Samba et al., 2020**); 12.4041 gm of cobalt nitrate, and 34.4369 gm of iron nitrate were weighed, and the resulting mixture was subsequently added to a small amount of distilled water. Additionally, 36.8486 gm of citric acid was added to the mixture, and 37.34 gm of ethylene diamine tetra acetic acid (EDTA) was added as a complication factor. An ammonia solution ($NH_3.H_2O$) was added to maintain the pH at 6, and the solution was evaporated using a heater while mixing with a magnetic mold to distribute heat. The mixture was stirred until a

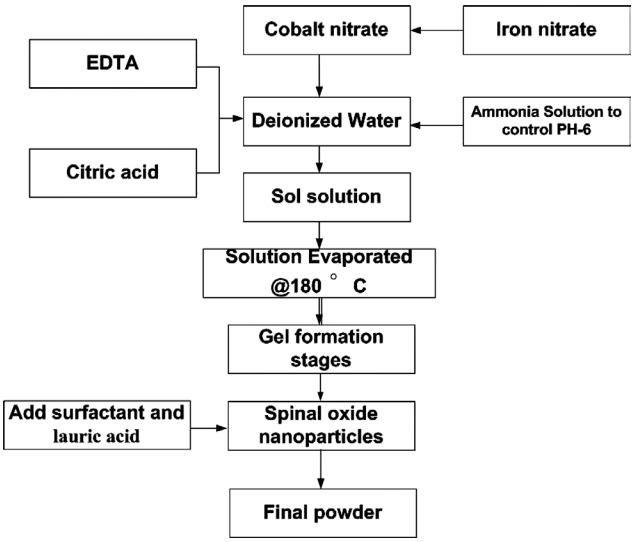

Figure 3: Step procedures to prepare the spinal oxide

Figure 4: Gel formation during the preparation

thick black gel formed, as shown in **Figure 4**. The magnetic stirrer was removed from the solution, allowing the gel to undergo thermal decomposition on the heater until it reached a fully combusted state, resulting in the formation of a solid material suitable for further thermal treatment. Subsequently, the resulting solid was transferred into a crucible and subjected to combustion in an oxidizing atmosphere within a furnace operating at 350°C for a duration of 5 hours. This process facilitated the elimination of residual organic constituents, yielding a refined powder consisting of cobalt ferrite oxide nanoparticles.

Generally, nanomaterial coated with lauric acid will be tested for the first time in the EOR section. However, spinel oxide NPs coated with both surfactant and lauric acid were prepared by mixing 70% spinel oxide with 30% surfactant and lauric acid in a solution containing 10% aqueous methanol warmed to 70°C (250 mL), followed by rinsing three times with hexane (3 × 50 mL). The resultant material was washed, with distilled water, vacuumed and dried at atmospheric pressure

overnight at 70°C in a hot air oven. The resulting material should ensure its capability to absorb the crude oil.

After preparing the coated CFO NPs, various characterization tests were conducted on the synthesized coated CFO NPs, including Fourier transform infrared spectroscopy (FTIR), X-ray fluorescence test (XRF), and X-ray powder diffraction (XRD), to confirm their nanomaterial properties. Subsequently, calculations of the capillary force restrictions between small and large oil droplets were calculated. Additionally, practical experiments involving oil droplets on glass plates at 30° were conducted for different scenarios: without water injection, with water injection, and during the CFO NPs absorption effect.

3. Results

3.1 Fourier Transform Infrared Spectroscopy (IR) Test for Coated Spinel Oxide

An IR test was conducted to analyse the functional groups on the surface of the coated CFO NPs prepared by the sol-gel method in air at 350°C for five hours, as mentioned above. The data were obtained using Fourier-transform infrared absorption spectrum FTIR. **Figure 5** displays the peaks of the FTIR results for coated CFO NPs, and it is readily visible that there are many peaks between the boundaries (3750 cm^{-1} and 670 cm^{-1}). The peaks at 3750 cm^{-1} and 2600 cm^{-1} can be attributed to the Fe-O and Co-O bonds, respectively. These characteristic peaks are attributed to all spinel oxides. In addition, the peak at 3490 cm^{-1} is attributed to the presence of water (H_2O) molecules. The infrared spectrum of the same sample revealed bands at 1480 and 1625 cm^{-1}, which could be attributed to υC=C (aromatic) and υ-COOH groups, respectively (**Samba et al., 2020**). The coating material exhibited similar infrared emissivities in most bands compared to previous IR tests for the same material prepared via the same procedures.

3.2 X-Ray Fluorescence (XRF) Test for Coated Spinel Oxide NPs

Table 1 presents the chemical composition of the coated CFO NPs. The table indicates that the prepared coated CFO NPs, in powder form, predominantly consist of iron (Fe) (44.78%) and cobalt (Co) (29.5%). This confirms the successful preparation process in acquiring the desired material. The presence of 29.5% oxygen (O) is associated with the oxide in the nanomaterial, namely cobalt ferrite oxide. Additionally, small amounts of other compositions such as sulfur (S), sodium (Na), magnesium (Mg), chlorine (Cl), etc. are also detected.

3.3. X-Ray Powder Diffraction (XRD) Test for Coated Spinel Oxide

Figure 6 displays the XRD pattern of the coated CFO NPs, obtained after burning the gel and obtaining the

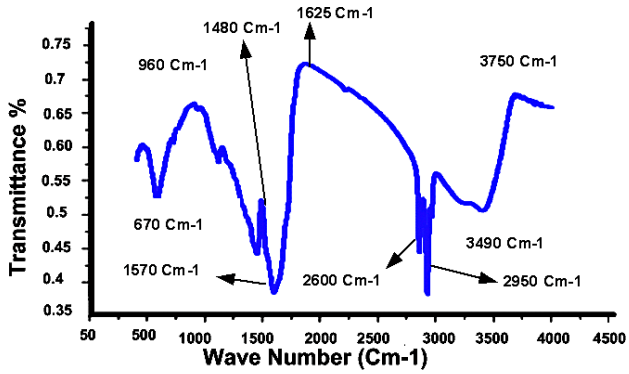

Figure 5: FTIR results for coated spinel oxide

Table 1: Chemical composition of coated spinel oxide

Compound	Concentration %
Fe	44.78
O	29.5
Co	23.57
S	0.858
Na	0.465
Cl	0.374
Ca	0.119
Si	0.105
Cu	0.088
Ni	0.043
Mg	0.03
Al	0.028
P	0.025
K	0.01

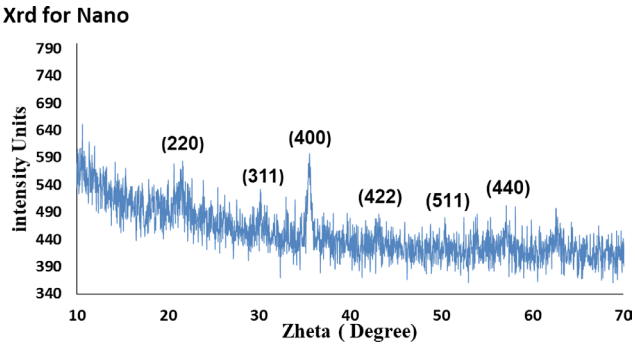

Figure 6: X-ray diffraction pattern of coated CFO NPs

solid form of the CFO NPs. The observed peaks corresponded well with the crystalline structure of the coated CFO NPs, matching the cubic structure (JCPDS card No. 22.0-1086.0). Notably, no additional peaks were observed in the XRD pattern besides those associated with the coated CFO NPs, confirming successful synthesis. The absence of peaks corresponding to the coated materials suggests they may have integrated into the spinel crystal lattice during high-temperature drying. The XRD pattern revealed characteristic reflection planes with

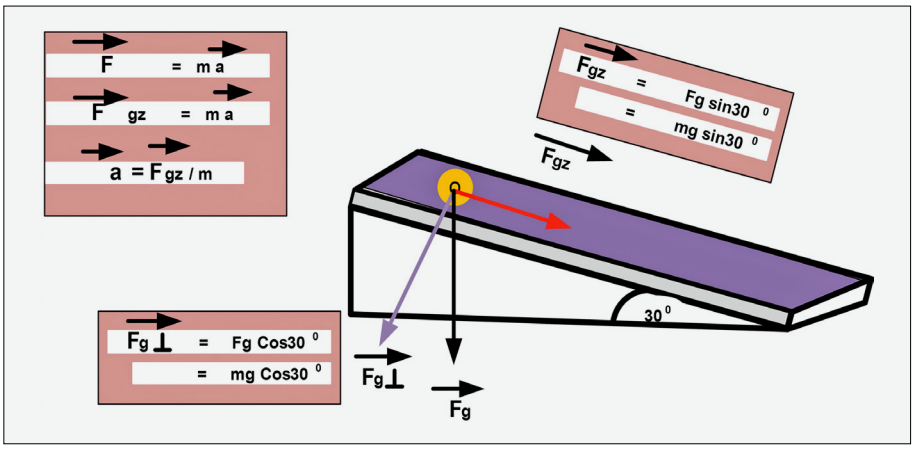

Figure 7: Small oil droplet analysis on the inclined surface

Miller indices of 220.0, 311.0, 422.0, 400.0, 511.0, 440.0, and 511.0 at 2θ values of 8.394°, 8.397°, 15.012°, 8.393°, 8.394°, 7.713° and 6.647°, respectively. Additionally, small impurities, represented by CoO and Fe_2O_3 were observed in the XRD pattern. The structural parameters of the coated CFO NPs, including lattice parameters such as X-Ray-Density (ρ XRD), unit cell volume (V cell), crystal size (D), and specific surface area (S XRD), were calculated from the XRD data obtained from the peak with high- intensity. The determined values were approximately 8.31600 Å, 579.7300 Å, 5.5200 g/cm^3, 28.31 nm, and 38.39 m^2/g for the a, V cell, ρ XRD, D, and S XRD, respectively.

3.4. Calculation of the capillary force restrictions based on the gravity force

3.4.1. Small oil droplet calculations

In this section, the forces acting on a small oil droplet weighing 0.0003 kg on the inclined surface at 30° are analysed, as depicted in **Figure 7**. The analysis is conducted based on the surface that lies on the oil droplet, with the different forces examined as follows:

- Perpendicular force ($(Fg)^{\sigma}$): gravity force mg.
- Vertical force ($(Fg^{\perp})^{\sigma}$)
- Horizontal force ($(Fgz)^{\sigma}$), which is parallel to the inclined surface.

Therefore,

For the vertical force

$$\left(\overrightarrow{Fg^{\perp}}\right) = F_g * \cos\theta \tag{1}$$

$$\left(\overrightarrow{Fg^{\perp}}\right) = mg * \cos\theta =$$

$$= 0.0003\,kg * 9.81\ m/s^2 * \cos 30° = 0.000453\,N$$

For horizontal force

$$(\overrightarrow{Fgz}) = F_g * \sin\theta \tag{2}$$

$$(\overrightarrow{Fgz}) = mg * \sin\theta =$$

$$= 0.0003\,kg * 9.81\ m/s^2 * \sin 30° = 0.0029\,N$$

Additionally, another force effecting on the oil droplet is the vertical force, which has the same magnitude but opposite directions as the vertical compound force $(Fg^{\perp})^{\sigma}$. The oil droplet will accelerate on the inclined surface because the vertical force on the inclined plate does not lead to acceleration on the body, due to the equal vertical compound force and vertical force.

Therefore, FN = - 0.000453 N

To calculate the acceleration of the oil droplet,

$$(\vec{F}) = m * (\vec{a}) \tag{3}$$

The force that causes the acceleration is $((Fgz)^{\sigma})$

$$(\overrightarrow{Fgz}) = m * (\vec{a}) \tag{4}$$

$$(\vec{a}) = \left(\frac{(\overrightarrow{Fgz})}{m}\right) \tag{5}$$

$$(\vec{a}) = \frac{0.0029\,N}{0.0003\,kg} = 9.666\,m/s^2$$

The assumption here is that the oil droplet is falling without any restrictions. Therefore, the acceleration is equal to 9.81 m/s^2 for the free movement of the oil droplet. However, based on the calculations, the accelerations have changed due to the movement restrictions. Consequently, it can be concluded that the capillary pressure restrictions on the movement are 9.81 - 9.66 = 0.14 m/s^2.

3.4.2. Large oil droplet calculations

In this section, the force analysis of a large oil droplet, weighing 0.0006 kg, positioned on the inclined surface at 30°, as depicted in **Figure 8**. Consequently, various

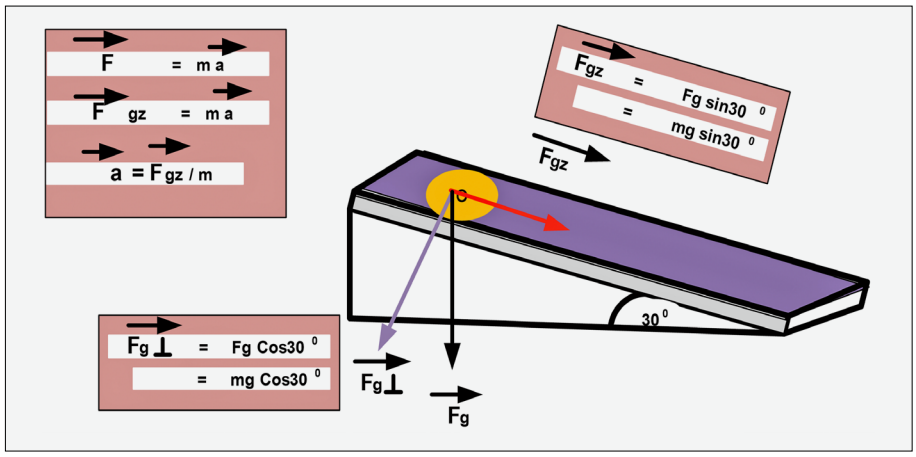

Figure 8: Large oil droplet analysis on the inclined surface

forces are analysed, similar to the scenario with the smaller oil droplet.

For the vertical force

$$\left(\overrightarrow{Fg^{\perp}}\right) = F_g * \cos\theta$$

$$\left(\overrightarrow{Fg^{\perp}}\right) = mg * \cos\theta =$$

$$= 0.0006\,\text{kg} * 9.81\ \text{m}/s^2 * \cos 30° = 0.000907\,\text{N}$$

For the horizontal force

$$(\overrightarrow{Fgz}) = F_g * \sin\theta$$

$$(\overrightarrow{Fgz}) = mg * \sin\theta =$$

$$= 0.0006\,\text{kg} * 9.8\ \text{m}/s^2 * \sin 30° = 0.00581\,\text{N}$$

As previously mentioned, another force effecting the oil droplet is vertical force, which has the same magnitude but opposite direction as the vertical compound force $(Fg^{\perp})^{\circlearrowright}$. The oil droplet will accelerate on the inclined surface because the vertical force on the inclined plate does not result in acceleration of the body due to the equal vertical compound force and vertical force.

Therefore, FN = – 0.000907 N

To calculate the acceleration of the oil droplet

$$(\vec{F}) = m * (\vec{a})$$

The force that causes the acceleration is $((Fgz)^{\circlearrowright})$

$$(\overrightarrow{Fgz}) = m * (\vec{a})$$

$$(\vec{a}) = \left(\frac{(\overrightarrow{Fgz})}{m}\right)$$

$$(\vec{a}) = \frac{0.0058\,\text{N}}{0.0006\,\text{kg}} = 9.683\,\text{m}/s^2$$

Hence, it can be concluded that the capillary pressure restrictions on the movement are 9.8 - 9.683 = 0.12 m/s^2.

Figure 9 illustrates a comparison of capillary pressure restrictions between oil droplets of different weights. The findings reveal that the large oil droplet has lower capillary pressure restrictions compared to the small oil droplet. Consequently, the chance of the larger oil droplet being free is more than of the smaller oil droplet.

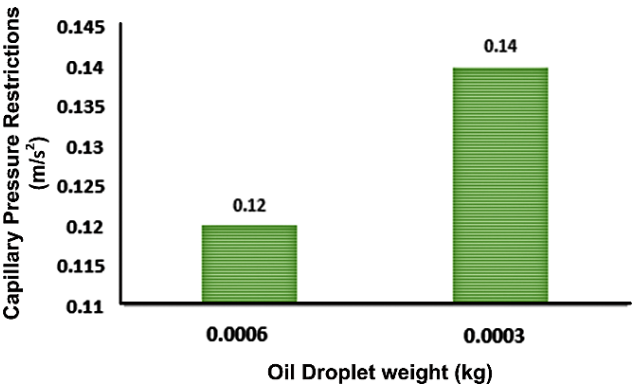

Figure 9: Capillary pressure restrictions

3.5. *Practical applications*

3.5.1. Oil droplet on the plate of glass at 30° without water injection

Two drops, each with different weights as previously analyzed, were positioned on a glass plate, as described above. Initially, the drops were placed on the plate at a flat position, as shown in **Figure 10**. Consequently, no movement or force is acting on the drop (the vertical force on the oil droplet is equal to the vertical compound force), and the drops are in a stable state. Subsequently, the plates were inclined at an angle of 30°, as shown in **Figure 11**, initiating movement in droplets due to the gravity force. The experiment revealed that the larger droplet moved more quickly than the the smaller droplet, as shown in **Figure 12**. This observation aligns with the results of the previous analysis (part 1 of this work (**Samba et al., 2023**)); emphasizing the significance of increasing the weight of the oil droplet for enhanced recovery.

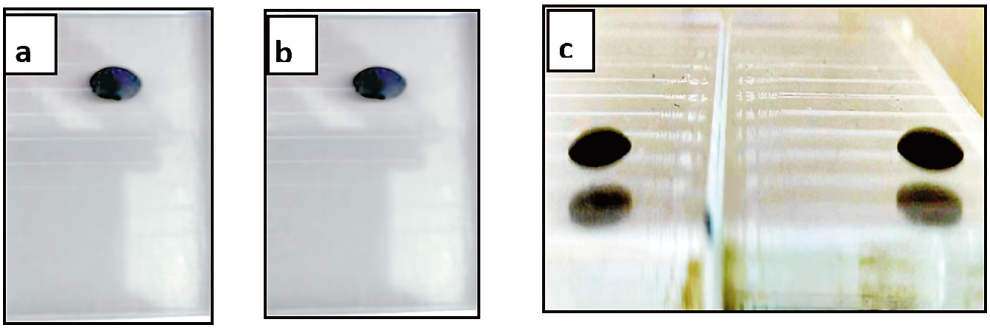

Figure 10: Oil droplets with different weights on the plate of glass;
a) small oil droplet, b) large oil droplet and c) small and large oil droplet on the flat plate

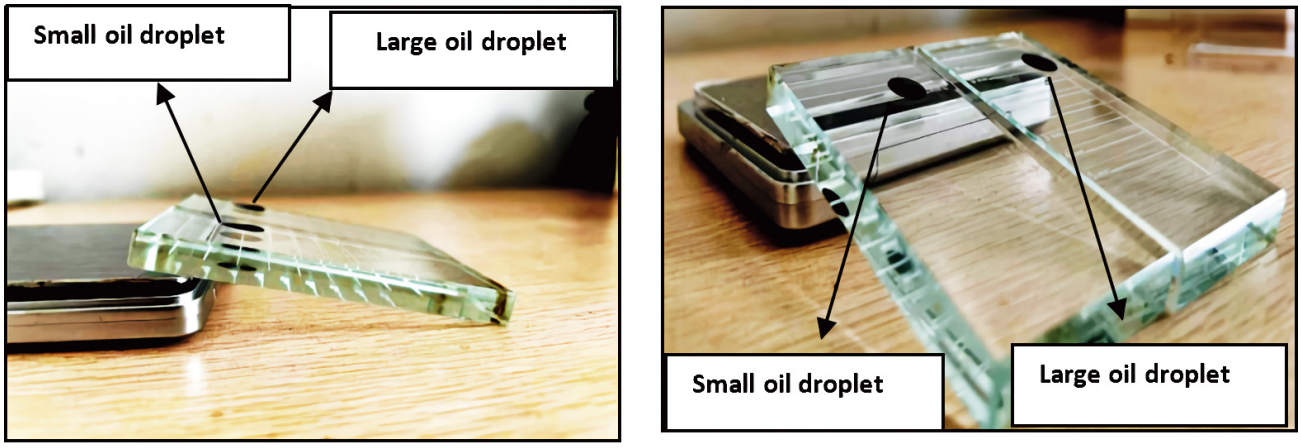

Figure 11: Oil droplets with different weights on the inclined plate of glass at 30°

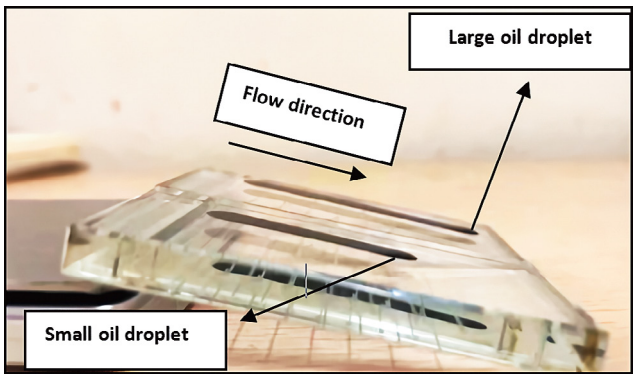

Figure 12: Acceleration difference between oil droplets

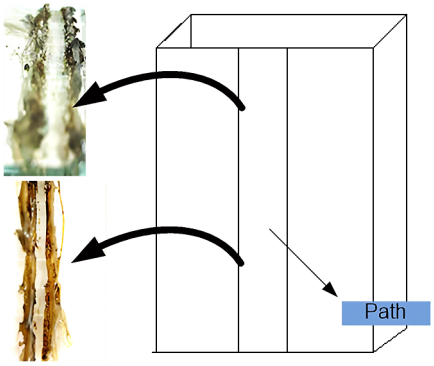

Figure 13: Path created on the glass plate

3.5.2. Oil droplet on the plate of glass at 30° during the water injection

A path was established on the glass plate, as shown in **Figure 13**, where the oil droplet was carefully positioned. In **Figure 14**, a passageway adjacent the oil droplet was created to investigate the behavior of the injected fluid when the oil droplet does not entirely fill the pore size. The water droplets were gradually increased, and their impact on the oil droplet was monitored. Initially, the water droplets encountered the oil droplet and attempted to displace it. However, due to the capillary force between the oil droplet and both the glass plate and

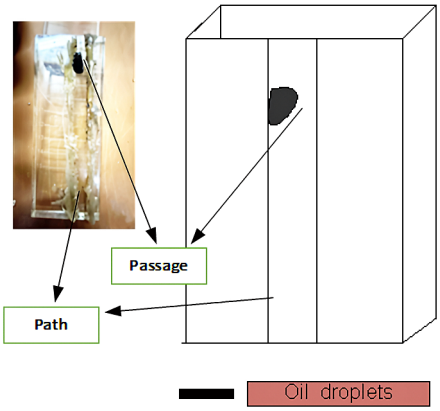

Figure 14: Placement of the oil droplet

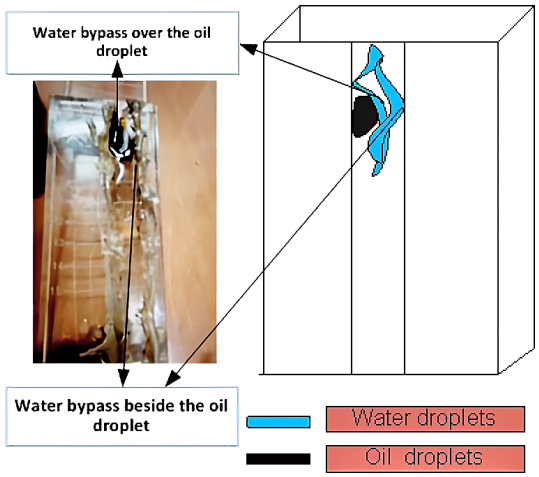

Figure 15: Water injection effect on the oil droplet in the case of present of bypassing conditions

the material forming the path, the water droplet failed to displace the oil droplet. Instead, the water droplet started to pass through the passageway beside and above the oil droplet, consistent with the increase in water droplets, as shown in **Figure 15**. This indicates the importance of the size of the oil droplet relative to the pore diameter, as explained in part 1 of this work (**Samba et al., 2023**).

3.5.3. Oil droplet on the plate of glass at 30° during the coated spinel oxide injection "absorption effect on the oil droplet"

Under the same conditions as in the previous scenario, water was replaced with the injection of a coated CFO NPs solution. The injection of the coated spinel oxide CFO NPs solution was gradually increased, and the impact of the coated spinel oxide solution droplets on the oil droplets was closely observed. Initially, as the coated spinel oxide solution encountered the oil droplet, attempts were made to displace it. Notably, the absorption of the coated CFO NPs onto the oil droplet was noticed, leading to the gathering of oil molecules and increasing the gravitational force acting on the oil droplet. This created favorable conditions for displacing the oil droplet. In this scenario, unlike water flooding, no water bypass beside the oil droplet was observed, highlighting a distinctive behavior associated with the injection of the coated spinel oxide solution.

While the absorption effect evident in previous tests, understanding the absorption phenomena in the EOR is considered fascinating. Thus far, understanding the oil droplet and the forces influencing it can facilitate a clear understanding of this phenomena. As seen above, the absorption phenomena result in the gathering of the oil droplets, preventing their bypass. As shown in **Figure 16**, the gathering of oil molecules enhances flow efficiency by preventing the bypass of the oil droplet. Additionally, the gathering of oil molecules induces corner flow, which can provide the suitable conditions to form

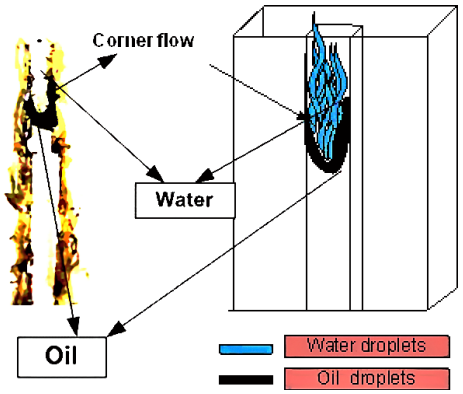

Figure 16: Absorption affects the oil droplet in the absence of bypassing conditions

the microemulsion. This gathering effect also influences the soaking time of oil droplets, a crucial factor in wettability alteration. The presented model suggests that corner flow has the potential to reduce injected pressure or enhance flow rates, thereby improving water flooding performance. This multifaceted understanding can contribute to optimizing EOR strategies.

Typically, in a state of rest with no external force acting on the oil droplet, the free surface of the liquid adopts a horizontal position. At this stage, different liquid particles experience only the force of gravity as a mass of force. However, when an external force is applied to push the oil droplet and absorption phenomena occur, the oil droplets start to accumulate and gather together, resulting in corner flow; the deformation of the oil phase surface progresses until a final parabolic form is observed, as shown in **Figure 17**. The analysis of the formed shape in the figure is as the follows:

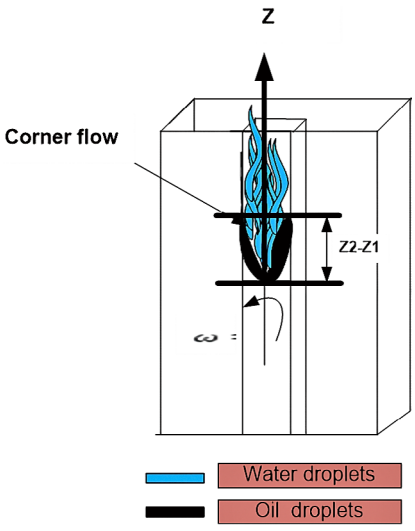

Figure 17: Corner flow that happened due to the absorption phenomena

$$\omega = 2\pi * n \tag{6}$$

$$a_r = -\omega^2 * r \tag{7}$$

Where:

ω = the rotation velocity (rad/sec),

n = number of rotation per second,

a_r = acceleration (m/s^2),

r = radius (m).

Applying Euler's equation in r direction (**Lacave et al., 2014**):

$$-\frac{\partial}{\partial r}(P+\gamma Z)=\rho * a_r \quad (8)$$

Substituting $a_r = -\omega^2 * r$

$$-\frac{\partial}{\partial r}(P+\gamma Z)=\rho * \omega^2 * r \quad (9)$$

$$\partial(P+\gamma Z)-\rho * \omega^2 * \partial r=0 \quad (10)$$

By integrating the previous equation (pressure form):

$$(P+\gamma Z)-\rho * \frac{\omega^2 * r^2}{2} = c \quad (11)$$

In addition, the head form can be obtained by dividing the previous equation by (head form):

$$\frac{P}{\gamma}+z-\frac{\omega^2 * r^2}{2g} = c \quad (12)$$

Based on the above equations, the surface profile of the corner flow can be calculated by using different rotation velocities, including 0.5, 0.4, 0.3, 0.2, and 0.1 rad/sec, each with a radius of 0.2 mm.

The following formula was applied:

$$\frac{P_1}{\gamma}+z_1-\frac{\omega^2 * r_1^2}{2g}=\frac{P_2}{\gamma}+z_2-\frac{\omega^2 * r_2^2}{2g} \quad (13)$$

$$z_2-z_1=\frac{\omega^2 * r_1^2}{2g} \quad (14)$$

Figure 18 shows the relationship between the oil deformation level vs rotational velocity. The results indicate that the deformation oil level increases with increasing of rotation velocity, and the corner flow can help increase the recovery factor.

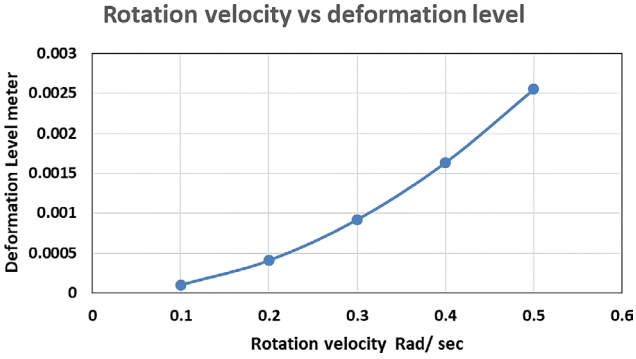

Figure 18: Rotations velocity vs deformation level

4. Discussions

The IR analysis revealed characteristic peaks corresponding to Fe-O and Co-O bonds, confirming the successful coating of CFO NPs. This characterization is vital for understanding the surface functional groups and chemical composition, which play a crucial role in the interaction between nanoparticles and oil droplets during EOR processes. Moreover, the elemental composition confirmed by XRF provided further evidence of the coating's integrity, primarily consisting of iron and cobalt, essential components for catalytic reactions in oil recovery processes. Additionally, the XRD patterns matched the expected cubic structure of coated CFO NPs, indicating successful synthesis and the absence of impurities, further supporting the suitability of these nanoparticles for EOR applications.

The analysis of oil droplet behaviour under gravitational and capillary forces offers valuable insight into fluid displacement mechanisms during EOR. The experiments conducted on inclined surfaces demonstrated that droplet size and weight significantly influence mobility and recovery efficiency. Larger oil droplets experienced lower capillary pressure restrictions, leading to enhanced mobility and potential for increased oil recovery. This observation underscores the importance of droplet characteristics in designing efficient EOR strategies.

The experimental setups simulating oil droplet movement on inclined surfaces provided practical implications for EOR applications. The injection of the coated spinel oxide solution showed promising results in enhancing oil displacement, attributed to the absorption effect leading to an increased gravitational force on oil droplets. This finding suggests that manipulating surface interactions through nanoparticle coatings could significantly improve recovery efficiency in EOR processes. Moreover, understanding absorption phenomena and corner flow dynamics presents opportunities for optimizing injection strategies and recovery performance in diverse reservoir conditions.

The findings from this study suggest several avenues for optimizing EOR strategies. By leveraging the insight gained from surface characterization and droplet behaviour analysis, researchers can develop tailored approaches to maximize oil recovery efficiency. Future research could focus on fine-tuning coating materials, optimizing injection parameters, and investigating the effects of fluid dynamics on recovery performance. Additionally, exploring the potential synergies between absorption phenomena and corner flow dynamics could lead to novel EOR techniques with enhanced effectiveness and sustainability.

5. Conclusions

This research has contributed to the advancement of knowledge in oil recovery mechanisms by investigating

the utilization of coated CFO nanoparticles. The experimental findings highlight the importance of augmenting oil droplet mass in later stages of production and reveal insight into capillary forces between small and large oil droplets. Notably, smaller droplets exhibit a greater capillary force, suggesting significant implications for oil-water interfacial dynamics. Additionally, the study elucidates the phenomenon of corner flow and its potential to alter the wettability of oil droplets through the aggregation of oil molecules via absorption phenomena. This observation underscores the relevance of understanding absorption phenomena in the context of oil recovery processes, paving the way for further research in this area. Acknowledging the study's limitations, particularly in experimental methodology, is crucial for interpreting the findings accurately. Future research endeavors should aim to address these limitations and explore the practical implications of absorption phenomena in oil recovery processes more comprehensively. In conclusion, this study lays a foundation for future investigations into absorption phenomena and its role in enhancing oil recovery strategies. By adopting a systematic approach to contextualize the findings within the broader landscape of enhanced oil recovery methods, researchers can advance the understanding of absorption phenomena's significance and potential applications in the field.

6. References

Agbalaka, C. C., Dandekar, A. Y., Patil, S. L., Khataniar, S., & Hemsath, J. R. (2009): Coreflooding studies to evaluate the impact of salinity and wettability on oil recovery efficiency. Transport in Porous Media, 76(1), 77–94. https://doi.org/10.1007/s11242-008-9235-7

Amar, I. A., Faraj, S., Abdulqadir, M., Abdalsamed, I., Altohami, F., & Samba, M. (2021): Oil spill removal from water surfaces using zinc ferrite magnetic nanoparticles as a sorbent material. Iraqi Journal of Science, 718–728.

Amar, I. A., Kanah, S. S., Hijaz, H. A., Abdulqadir, M. A., Shamsi, S. A., Abdalsamed, I. A., & Samba, M. A. (2023): Surfactant-assisted sol-gel synthesis of zinc ferrite magnetic nanoparticles for oil spills cleanup from seawater and antibacterial activity applications. World Journal of Engineering, 20(4), 713–721.

Andersen, P. Ø. (2020): Capillary Pressure Effects on Estimating the Enhanced-Oil-Recovery Potential During Low-Salinity and Smart Waterflooding. SPE Journal, 25(01), 481–496. https://doi.org/10.2118/191974-PA

Esfe, M. H., Esfandeh, S., & Hosseinizadeh, E. (2020): Nanofluid flooding in a randomized heterogeneous porous media and investigating the effect of capillary pressure and diffusion on oil recovery factor. Journal of Molecular Liquids, 320, 113646. https://doi.org/10.1016/j.molliq.2020.113646

Green, D. W., & Willhite, G. P. (1998): Enhanced oil recovery (Vol. 6). Henry L. Doherty Memorial Fund of AIME, Society of Petroleum Engineers.

Janssen, P. H., Van Den Broek, W., & Harris, C. K. (2001): Laboratory study investigating emulsion formation in the near-wellbore region of a high water-cut oil well. SPE Journal, 6(01), 71–79.

Lacave, C., Miot, E., & Wang, C. (2014): Uniqueness for the two-dimensional Euler equations on domains with corners. Indiana University Mathematics Journal, 1725–1756.

Massoud, M. A. E., Li, Y., & Amar, I. A. (2022): Literature Review of Nanotechnology in the Enhanced Oil Recovery. Journal of Engineering Research.

Nobakht, M., Moghadam, S., & Gu, Y. (2007): Effects of viscous and capillary forces on CO_2 enhanced oil recovery under reservoir conditions. Energy & Fuels, 21(6), 3469–3476. https://doi.org/10.1021/ef700388a.

Pradhan, P., Giri, J., Banerjee, R., Bellare, J., & Bahadur, D. (2007): Cellular interactions of lauric acid and dextran-coated magnetite nanoparticles. Journal of Magnetism and Magnetic Materials, 311(1), 282–287.

Rai, K., Johns, R. T., Delshad, M., Lake, L. W., & Goudarzi, A. (2013): Oil-recovery predictions for surfactant polymer flooding. Journal of Petroleum Science and Engineering, 112, 341–350.

Romanuka, J., Hofman, J., Ligthelm, D. J., Suijkerbuijk, B., Marcelis, F., Oedai, S., Brussee, N., van der Linde, H., Aksulu, H., & Austad, T. (2012): Low salinity EOR in carbonates. SPE Improved Oil Recovery Symposium. https://doi.org/10.2118/153869-MS

Rossen, W. R., & Lu, Q. (1997): Effect of capillary crossflow on foam improved oil recovery. SPE Western Regional Meeting. https://doi.org/10.2118/38319-MS

Samba, M. A., Amar, I. A., Abuadabba, M., ALfroji, M. A., Salih, Z. M., & Erfando, T. (2020): Separation of Crude Oil and Its Derivatives Spilled in Seawater by using Cobalt Ferrite Oxide.

Samba, M. A., Hassan, H. A., Munayr, M. S., Yusef, M., Eschweido, A., Burkan, H., & Elsharafi, M. O. (2019): Nanoparticles EOR aluminum oxide (Al_2O_3) used as a spontaneous imbibition test for sandstone core. ASME International Mechanical Engineering Congress and Exposition, Proceedings (IMECE). https://doi.org/10.1115/IMECE2019-10283

Samba, M. A., Li, Y., liu, Z., Almahdi, A. S., & Siregar, H. P. S. (2023): The effect of forces affecting the spread of oil droplets on a rock surface. Journal of Petroleum Exploration and Production Technology, 1–8.

Sun, X., Zhang, Y., Chen, G., & Gai, Z. (2017): Application of nanoparticles in enhanced oil recovery: a critical review of recent progress. Energies, 10(3), 345.

Tola, S., Sasaki, K., & Sugai, Y. (2017): Wettability alteration of sandstone with zinc oxide nano-particles. 23rd Formation Evaluation Symposium of Japan.

SAŽETAK

Istraživanje učinka apsorpcije na naftne kapljice u povećanju iscrpka nafte: pristup analize sila

U ovome su istraživanju analizirane sile koje utječu na kapljice nafte, kako bi se pokazalo da povećanje mase naftne kapljice stvara povoljne uvjete za interakciju između fluida koji se istiskuje i fluida koji se koristi za istiskivanje. To posljedično dovodi do smanjenja zaobilaženja fluida za istiskivanje oko kapljica nafte. U ovome je istraživanju povećanje mase kapljice nafte postignuto apsorpcijom, korištenjem obloženih nanočestica spinel oksida (kobalt-ferit, CFO nanočestice). Sinteza CFO nanočestica uspješno je provedena u laboratoriju primjenom postupka sol-gel, nakon čega je uslijedilo oblaganje surfaktantom i laurinskom kiselinom. Djelovanje obloženih nanočestica spinel oksida istraženo je pomoću IR, XRD i XRF postupaka. Postupak karakterizacije započeo je proračunom ograničenja kapilarne sile za male i velike kapljice nafte. Također, napravljeni su i eksperimenti s kapljicama nafte na staklenim pločicama postavljenim pod kutom od 30° za različite scenarije: bez utiskivanja vode, s utiskivanjem vode i uz primjenu CFO nanočestica, tj. s efektom apsorpcije CFO nanočestica. Istraživanja su pokazala da velika naftna kapljica ima manja ograničenja izazvana kapilarnim tlakom u odnosu na male kapljice nafte, s razlikom od 0,02 m/s^2. Posljedica je toga lakše oslobađanje većih kapljica nafte u odnosu na male. Nadalje, u slučaju kada nema utiskivanja, velika kapljica nafte pokazuje brže kretanje od male kapljice nafte zbog utjecaja gravitacije. Tijekom scenarija utiskivanja vode kapljice vode nisu mogle istisnuti kapljicu nafte; umjesto toga one su prolazile oko kapljice nafte povećavajući količinu vode u iscrpku. Međutim, u scenariju u kojemu su korištene CFO nanočestice primijećena je apsorpcija obloženih CFO nanočestica na kapljicu nafte. To je rezultiralo nakupljanjem molekula nafte što je povećalo težinu naftne kapljice i stvorilo povoljne uvjete za njezino istiskivanje. Bitno je da u ovome scenariju, za razliku od scenarija s utiskivanjem vode, nije zamijećeno zaobilaženje kapljica nafte vodom. Dodatno, nakupljanje molekula nafte potaknulo je protjecanje fluida uz kutove (engl. *corner flow*), čime su stvoreni povoljni uvjeti za stvaranje mikroemulzije, promjene močivosti, mijenjanja rezidualnoga zasićenja naftom i povećanja učinkovitosti utiskivanja. Za analizu kutnoga protoka korištena je Eulerova jednadžba, koja je pokazala da se razina deformacije naftne kapljice povećava s povećanjem brzine rotacije, što potencijalno dovodi do povećanja iscrpka.

Ključne riječi:
kapljica nafte, gravitacijska sila, kapilarna sila, protjecanje fluida uz kutove, nanočestica spinel oksida

Author's Contribution

Mohammed A. Samba (1) (PhD Candidate at China University of Petroleum, Beijing, currently a member of the Petroleum staff at Sebha University) Conceptualization, methodology, writing - original draft preparation, writing - review, editing, and project Administration. **Yiqiang Li (2)** (Head of Oil and Gas Lab at CUPB) Supervision, methodology, writing - review, editing, and data curation. **Zheyu Liu (3)** (Assistant of the Head of Oil and Gas Lab at CUPB) Provision of materials, laboratory facilities, and formal analysis. **Ibrahim A. Amar (4)** (Member of Chemical Science staff at Sebha University) Supervision of nano preparation and characterization, investigation, resources, and data curation. **Muslim Abdurrahman (5)** (Dean of Engineering Faculty at Universitas Islam Riau) Visualization, data curation, and formal analysis. **Peter O. Anyimah (6)** (PhD Candidate at China University of Petroleum, Beijing) Writing - review, editing, visualization, and resources.